Selected Topics of High Speed Machining Analysis[*]

Tomasz ŁODYGOWSKI[1], Alexis RUSINEK[2], Tomasz JANKOWIAK[1],
Wojciech SUMELKA[1]

[1] *Poznan University of Technology*
Faculty of Civil and Environmental Engineering
Institute of Structural Engineering

Piotrowo 5, 60-965 Poznań, Poland
e-mail: {Tomasz.Lodygowski, Tomasz.Jankowiak, Wojciech.Sumelka}@put.poznan.pl

[2] *National Engineering School of Metz (ENIM)*
Laboratory of Mechanics, Biomechanics, Polymers and Structures (LaBPS)

1 route d'Ars Laquenexy, 57000 Metz, France
e-mail: Rusinek@enim.fr

Some aspects of numerical analysis of problems related to high strain rates with thermal effects are considered. The attention is focused on constitutive modelling that describes the accompanied phenomena like plastic strain localization and softening. The importance of proper formulation of failure criteria is stressed. Also the complexity of computations is discussed.

Key words: high speed machining, numerical simulation, plasticity and softening.

1. INTRODUCTION

The high speed processes that generate rates of deformation of order 10^4–10^7 s^{-1} for ductile and brittle materials are still in focus of interests. There are crucial for those who work on constitutive modeling as well as computations. These two areas have to be carefully investigated. In particular, when we face the problems of softening due to fundamental thermal effects one can expect the difficulties connected with mathematical well posedness of the boundary value problems and in consequence the uniqueness of the obtained results. This effect appears when non-positive constitutive stiffness follows the overcoming of local peak in stress-strain space. In classical plasticity formulation the consequences of softening drive to lose of the type of the governing set of differential equa-

---

[*] Initial lecture for VIII International Conference HIGH SPEED MACHINING, December 08-10, 2010, Metz, France.

tions and this requires a regularization. It can be done in different manner: 1) on the level of mathematical formulation of constitutive relations (rate dependent viscoplastic models, higher order gradient etc) or 2) on the level of numerical applications (introducing the localization zones into the approximation). Both those treatments we believe could be successful and the results for some particular cases are comparable with the real behavior of the matter, however only this which has the strong physical background should be acceptable.

2. Selected constitutive models

2.1. General remarks

The constitutive formulations which introduce the rate dependence have a chance for regularization of initial value problems and in consequence, after numerical discretization, can reproduce the behavior with a proper accuracy.

There are some main constitutive formulations commonly used which serve to describe the behavior of ductile materials including plastic strain localization and thermal softening. These constitutive models introduce implicitly or explicitly the internal length scale which plays the role of regularization parameter. These formulations will be discussed. The discussion will be focused on viscoplastic (eg. Perzyna's type) but also Rusinek–Klepaczko models which will be compared with commonly used and applied in numerical codes like Johnson-Cook one. Let stress that we focus our attention onto fast dynamic processes. The governing set of equations is of hyperbolic type until the softening effects are not present. The speed of the process is measured rather by the rate of stains than by the velocity of the movements. The process under consideration has to describe the strain localization followed by local fracture, development of cracks and finally the failure of the specimen.

2.2. Johnson-Cook model

Let us start with the well established constitutive model proposed by John-son and Cook (JC) [5] and shortly remind the its well known properties. The JC model allows to take into account hardening, strain rate and temperature sensitivity. The explicit formulation of the JC model is defined as follows

$$(2.1) \qquad \sigma(\varepsilon_{pl}, \dot{\varepsilon}_{pl}, T) = (A + B\varepsilon_{pl}^n) \left[1 + C \ln\left(\frac{\dot{\varepsilon}_{pl}}{\dot{\varepsilon}_0} \right) \right] \left[1 - \left(\frac{T - T_0}{T_{\text{melt}} - T_0} \right)^m \right],$$

where A is a yield stress, B and n are strain hardening coefficients, C is a strain rate sensitivity coefficient and m describes the temperature sensitivity. To define the thermal softening of the material during dynamic loading, the heat equation

is used. It allows to compute the temperature rise based on the quantity of plastic work converted into heat

$$(2.2) \qquad \Delta T(\varepsilon, \dot{\varepsilon}) = \frac{\beta}{\rho C_p} \int\limits_{\varepsilon^e}^{\varepsilon^{\max}} \sigma d\varepsilon^{pl},$$

where β is the Quinney–Taylor coefficient proportional to the quantity of plastic work converted into heat, ρ is a density of the material and C_p is a specific heat. Thus the current temperature T is defined as

$$(2.3) \qquad T(\varepsilon^{pl}, \dot{\varepsilon}) = T_0 + \Delta T(\varepsilon^{pl}, \dot{\varepsilon}),$$

where T_0 is the initial temperature. So to describe any material (metal) one has to identify 5 constitutive parameters except of knowing its physical constants.

Because of its relative simplicity JC model is widely used in many engineering applications however in comparison with experiments it underestimates the results for very high strain rates. The constitutive model is implemented in Abaqus/Explicit environment and will be used for comparison with the other discussed models.

2.3. Rusinek–Klepaczko model

To describe the thermoviscoplastic behaviour of mild steel, an original constitutive relation has been used which couples hardening, temperature and strain rate sensitivity. However, it allows to take into account the non linearity in term of strain rate and temperature sensitivity. The equivalent stress $\sigma(\varepsilon^{pl}, \dot{\varepsilon}^{pl}, T)$ is an addition of two components, the internal stress $\sigma_\mu(\varepsilon^{pl}, \dot{\varepsilon}^{pl}, T)$ and the effective stress $\sigma^*(\dot{\varepsilon}^{pl}, T)$. The first one describes the hardening and the second one, the sensitivity and the reciprocity between strain rate and temperature. It base mainly on the Arrhenius equation. Due to the microstructure of the material, BCC, an additive decomposition is used, Eq. (2.4) allowing for a better description [7, 23, 28]

$$(2.4) \qquad \sigma(\varepsilon^{pl}, \dot{\varepsilon}^{pl}, T) = \frac{E(T)}{E_0} \left[\sigma_\mu(\varepsilon^{pl}, \dot{\varepsilon}^{pl}, T) + \sigma^*(\dot{\varepsilon}^{pl}, T) \right],$$

where $E(T)$ is the Young's modulus depending on temperature and E_0 is the Young's modulus at $T = 0$ K.

The Young's modulus itself is defined as follows Eq. (2.5),

$$(2.5) \qquad E(T) = E_0 \left\{ 1 - \frac{T}{T_m} \exp\left[\theta^* \left(1 - \frac{T_m}{T} \right) \right] \right\},$$

where θ^* is a material constant depending of the microstructure. For ferritic steel $\theta^* = 0.59$ and for austenitic steel $\theta^* = 0.9$ as discussed in [26].

The explicit relations for the internal stresses $\sigma_\mu(\varepsilon^{pl}, \dot{\varepsilon}^{pl}, T)$ and the effective stresses $\sigma^*(\dot{\varepsilon}^{pl}, T)$ are the following, Eqs. (2.6) and (2.7)

$$(2.6) \qquad \sigma_\mu(\varepsilon^{pl}, \dot{\varepsilon}^{pl}, T) = B(\dot{\varepsilon}^{pl}, T)(\varepsilon_0 + \varepsilon^{pl})^{n(\dot{\varepsilon}^{pl}, T)},$$

$$(2.7) \qquad \sigma^*(\dot{\varepsilon}^{pl}, T) = \sigma_0^* \left\langle 1 - D_1 \left(\frac{T}{T_m}\right) \log\left(\frac{\dot{\varepsilon}_{\max}}{\dot{\varepsilon}^{pl}}\right) \right\rangle^{m^*},$$

where $B(\dot{\varepsilon}^{pl}, T)$ is the modulus of plasticity proportional to the yield stress and depends on strain rate and temperature. The exponent $n(\dot{\varepsilon}^{pl}, T)$ is the hardening coefficient which depends on strain rate and temperature and allows to define properly thermal softening during plastic deformation. D_1 is a material constant, T_m is the melting temperature, σ_0^* is a constant of the material, m^* is the strain rate sensitivity parameter. ε_0 is a material constant allowing to adjust the yield stress and $\dot{\varepsilon}_{\max} = 10^7$ s^{-1} is the maximum strain rate allowed for model based on experiments.

The explicit expressions for $n(\dot{\varepsilon}^{pl}, T)$ and $B(\dot{\varepsilon}^{pl}, T)$ are defined by Eqs. (2.8) and (2.9)

$$(2.8) \qquad n(\dot{\varepsilon}^{pl}, T) = n_0 \left\langle 1 - D_2 \left(\frac{T}{T_m}\right) \log\left(\frac{\dot{\varepsilon}^{pl}}{\dot{\varepsilon}_{\min}}\right) \right\rangle,$$

$$(2.9) \qquad B(\dot{\varepsilon}^{pl}, T) = B_0 \left\langle \frac{T}{T_m} \log\left(\frac{\dot{\varepsilon}_{\max}}{\dot{\varepsilon}^{pl}}\right) \right\rangle^{-\nu_{CR}},$$

where $\dot{\varepsilon}_{\min} = 10^{-5}$ s^{-1} is the lower strain rate limit of the model, ν_{CR} is the temperature sensitivity coefficient, D_2, B_0 and n_0 are the constants for the material studied.

In addition, this model called RK has been developed originally with an algorithm allowing to define in a precise way all the constants of the model [7]. Therefore, the constants are independent of the user and the set of constants is unique for each material. The constants are defined step by step following physical restrictions. This model is used with success to describe the behaviour of different materials [24–26].

2.4. Perzyna's type viscoplasticity model

2.4.1. Introductory remarks

The material model is stated in the framework of the thermodynamical theory of viscoplasticity together with a phenomenological approach [4, 22, 32]. Formally, the constitutive structure belongs to the class of simple materials with fading memory. Due to its final form and the way of incorporating the fundamental variables, it also belongs to the class of rate dependent material with

internal state variables [33]. Such an approach locates the model in the macro (meso-macro) space scale, thus all variables in the model reflect the homogenised reactions from smaller scales.

Let us shortly describe the key features of mathematical model for adiabatic process (for detailed and more general formulation see [31]). They are: (i) the description is invariant with respect to any diffeomorphism, (ii) the obtained evolution problem is well-posed, (iii) sensitivity to the rate of deformation, (iv) finite elasto-viscoplastic deformations, (v) plastic non-normality, (vi) dissipation effects, (vii) thermo-mechanical couplings and (viii) length scale sensitivity. It should be emphasised also that every variable in the model has a physical interpretation derived from analysis of single crystal and polycrystal behaviour.

In the discussed model, an important role plays the description of damage. We introduce the second order microdamage tensorial field (as a state variable), denoted by ξ, cf. [4, 22, 31], which reflects the experimentally observed anisotropy of metals in the mathematical (constitutive) model. Such approach enables us to keep good global damage approximation (GDA) (strain-stress curves fitting from experiment and mathematical model) but especially good local damage approximation (LDA) (GDA plus coincidence in: macrodamage initiation time, velocity of macrodamage evolution and the geometry of macrodamage pattern). Let us emphasise that the Euclidean norm of the microdamage field defines the scalar quantity called the *volume fraction porosity* or simply *porosity* [22] while its principal values are proportional to the ratio of the damaged area to the assumed characteristic area of the representative volume element [31], thus they indicate damage plane as one perpendicular to maximal principal value of ξ (cf. Fig. 1).
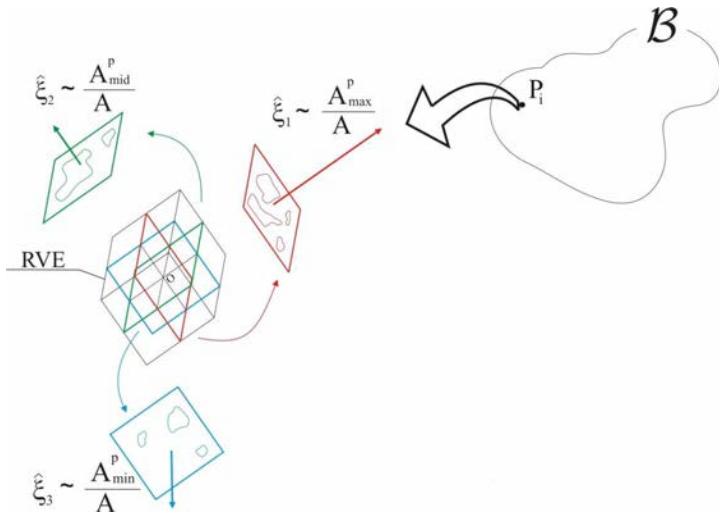

Fig. 1. The concept of microdamage tensor.

2.4.2. *Adiabatic process*

Kinematics. The abstract body is a differential manifold. The kinematics of the finite elasto-viscoplastic deformations is governed by the multiplicative decomposition of the total deformation gradient to the elastic and viscoplastic parts [8]

$$(2.10) \qquad \mathbf{F}(\mathbf{X}, t) = \mathbf{F}^e(\mathbf{X}, t) \cdot \mathbf{F}^p(\mathbf{X}, t),$$

where $\mathbf{F} = \dfrac{\partial \phi(\mathbf{X}, t)}{\partial \mathbf{X}}$ is the deformation gradient, ϕ describes the motion, $\mathbf{X}$ denotes material coordinates, t is time and $\mathbf{F}^e$, $\mathbf{F}^p$ are elastic and viscoplastic parts, respectively.

From the spatial deformation gradient, denoted by $\mathbf{l}$,

$$(2.11) \qquad \mathbf{l}(\mathbf{x}, t) = \frac{\partial \boldsymbol{\upsilon}(\mathbf{x}, t)}{\partial \mathbf{x}},$$

where $\boldsymbol{\upsilon}$ denotes spatial velocity and $\mathbf{x}$ are spatial coordinates, we obtain

$$(2.12) \qquad \mathbf{l} = \mathbf{d} + \mathbf{w} = \mathbf{d}^e + \mathbf{w}^e + \mathbf{d}^p + \mathbf{w}^p,$$

$$(2.13) \qquad \mathbf{d} = \frac{1}{2}(\mathbf{l} + \mathbf{l}^T),$$

$$(2.14) \qquad \mathbf{w} = \frac{1}{2}(\mathbf{l} - \mathbf{l}^T),$$

where $\mathbf{d}$ is the symmetric part and $\mathbf{w}$ is the antisymmetric part, of $\mathbf{l}$, respectively. Now, assuming that the Euler–Almansi strain is taken as a strain measure and applying Lie derivative we have the fundamental relation

$$(2.15) \qquad \mathbf{d}^\flat = \mathrm{L}_{\boldsymbol{\upsilon}}(\mathbf{e}^\flat),$$

and simultaneously

$$(2.16) \qquad \mathbf{d}^{e\flat} = \mathrm{L}_{\boldsymbol{\upsilon}}(\mathbf{e}^{e\flat}), \qquad \mathbf{d}^{p\flat} = \mathrm{L}_{\boldsymbol{\upsilon}}(\mathbf{e}^{p\flat}),$$

where $\mathrm{L}_{\boldsymbol{\upsilon}}$ stands for Lie derivative, $\mathbf{e}$ for the Euler–Almansi strain and $\flat$ indicates the tensor that has all its indices lowered. These relations show that the symmetric part of spatial deformation gradient $\mathbf{d}$ is directly Lie derivative of the Euler–Almansi strain.

Constitutive postulates [19]. Assuming that the balance principles hold: conservation of mass, balance of momentum, balance of moment of momentum and balance of energy and entropy production, we define four constitutive postulates [21]:

(i) Existence of the free energy function ψ. Formally we apply it in the following form

$$(2.17) \qquad \psi = \widehat{\psi}(\mathbf{e}, \mathbf{F}, \vartheta; \boldsymbol{\mu}),$$

where $\boldsymbol{\mu}$ denotes a set of internal state variables governing the description of dissipation effects and ϑ denotes temperature.

(ii) Axiom of objectivity (spatial covariance). The material model should be invariant with respect to any superposed motion (diffeomorphism).

(iii) The axiom of the entropy production. For every regular process the constitutive functions should satisfy the second law of thermodynamics.

(iv) The evolution equation for the internal state variables vector $\boldsymbol{\mu}$ should be of the form

$$(2.18) \qquad \mathrm{L}_{\boldsymbol{\upsilon}}\boldsymbol{\mu} = \widehat{\mathbf{m}}(\mathbf{e}, \mathbf{F}, \vartheta, \boldsymbol{\mu}),$$

where evolution function $\widehat{\mathbf{m}}$ has to be determined based on the experimental observations.

Initial boundary value problem. Under the above conditions the deforming body under adiabatic regime is governed by the following set of equations. They state the initial boundary value problem (IBVP).

Find ϕ, $\boldsymbol{\upsilon}$, ρ, $\boldsymbol{\tau}$, $\boldsymbol{\xi}$, ϑ as functions of t and position $\mathbf{x}$ such that [9, 11, 12, 20]:

(i) the field equations

$$
\begin{aligned}
&\dot{\phi} = \boldsymbol{\upsilon}, \\
&\dot{\boldsymbol{\upsilon}} = \frac{1}{\rho_{\mathrm{Ref}}}\left(\mathrm{div}\boldsymbol{\tau} + \frac{\boldsymbol{\tau}}{\rho}\cdot\mathrm{grad}\rho - \frac{\boldsymbol{\tau}}{1-(\boldsymbol{\xi}:\boldsymbol{\xi})^{1/2}}\mathrm{grad}(\boldsymbol{\xi}:\boldsymbol{\xi})^{1/2}\right), \\
&\dot{\rho} = -\rho\,\mathrm{div}\boldsymbol{\upsilon} + \frac{\rho}{1-(\boldsymbol{\xi}:\boldsymbol{\xi})^{1/2}}(\mathrm{L}_{\boldsymbol{\upsilon}}\boldsymbol{\xi}:\mathrm{L}_{\boldsymbol{\upsilon}}\boldsymbol{\xi})^{1/2}, \\
(2.19)\quad &\dot{\boldsymbol{\tau}} = \mathcal{L}^e:\mathbf{d} + 2\boldsymbol{\tau}\cdot\mathbf{d} - \mathcal{L}^{th}\dot{\vartheta} - (\mathcal{L}^e + \mathbf{g}\boldsymbol{\tau} + \boldsymbol{\tau}\mathbf{g}):\mathbf{d}^p, \\
&\dot{\boldsymbol{\xi}} = 2\boldsymbol{\xi}\cdot\mathbf{d} + \frac{\partial g^*}{\partial\boldsymbol{\tau}}\frac{1}{T_m}\left\langle \Phi^g\left[\frac{I_g}{\tau_{eq}(\boldsymbol{\xi},\vartheta,\in^p)} - 1\right]\right\rangle, \\
&\dot{\vartheta} = \frac{\chi^*}{\rho c_p}\boldsymbol{\tau}:\mathbf{d}^p + \frac{\chi^{**}}{\rho c_p}\mathbf{k}:\mathrm{L}_{\boldsymbol{\upsilon}}\boldsymbol{\xi},
\end{aligned}
$$

(ii) the boundary conditions

   (a) displacement ϕ is prescribed on a part Γ_ϕ of $\Gamma(\mathcal{B})$ and tractions $(\boldsymbol{\tau} \cdot \mathbf{n})^a$ are prescribed on a part Γ_τ of $\Gamma(\mathcal{B})$, where $\Gamma_\phi \cap \Gamma_\tau = 0$ and $\Gamma_\phi \cup \Gamma_\tau = \Gamma(\mathcal{B})$,

   (b) heat flux $\mathbf{q} \cdot \mathbf{n} = 0$ is prescribed on $\Gamma(\mathcal{B})$,

(iii) the initial conditions $\phi, \boldsymbol{\upsilon}, \rho, \boldsymbol{\tau}, \boldsymbol{\xi}, \vartheta$ are given for each particle $\mathbf{X} \in \mathcal{B}$ at $t = 0$,

are satisfied. In above, we have denoted: ρ_{Ref} as a referential density, $\boldsymbol{\tau}$ as the Kirchhoff stress tensor, ρ as a current density, $\mathcal{L}^e$ as an elastic constitutive tensor, $\mathcal{L}^{th}$ as a thermal operator, $\mathbf{g}$ as a metric tensor, $\partial g^*/\partial \boldsymbol{\tau}$ as the evolution directions for anisotropic microdamage growth processes, T_m as a relaxation time of mechanical disturbances, I_g as a stress intensity invariant, τ_{eq} as the threshold stress, χ^*, χ^{**} as the irreversibility coefficients and c_p as a specific heat.

Material functions. For the evolution problem (2.19) we assume the following:

1. For elastic constitutive tensor $\mathcal{L}^e$

$$(2.20) \qquad \mathcal{L}^e = 2\mu \mathcal{I} + \lambda(\mathbf{g} \otimes \mathbf{g}),$$

   where μ, λ are Lamé constants.

2. For thermal operator $\mathcal{L}^{th}$

$$(2.21) \qquad \mathcal{L}^{th} = (2\mu + 3\lambda)\theta\mathbf{g},$$

   where θ is thermal expansion coefficient.

3. For viscoplastic flow phenomenon $\mathbf{d}^p$ [16, 17]

$$(2.22) \qquad \mathbf{d}^p = \Lambda^{vp}\mathbf{p},$$

   where

$$(2.23) \qquad \Lambda^{vp} = \frac{1}{T_m}\left\langle \Phi^{vp}\left(\frac{f}{\kappa} - 1\right)\right\rangle = \frac{1}{T_m}\left\langle \left(\frac{f}{\kappa} - 1\right)^{m_{pl}}\right\rangle,$$

$$(2.24) \qquad f = \left\{ J_2' + \left[n_1(\vartheta) + n_2(\vartheta)(\boldsymbol{\xi} : \boldsymbol{\xi})^{1/2}\right] J_1^2 \right\}^{1/2},$$

$$(2.25) \qquad n_1(\vartheta) = 0, \qquad n_2(\vartheta) = n = \text{const.},$$

(2.26) $\kappa = \{\kappa_s(\vartheta) - [\kappa_s(\vartheta) - \kappa_0(\vartheta)] \exp\left[-\delta(\vartheta) \in^p\right]\}$

$$\cdot \left[1 - \left(\frac{(\boldsymbol{\xi} : \boldsymbol{\xi})^{1/2}}{\xi_F}\right)^{\beta(\vartheta)}\right],$$

(2.27) $\overline{\vartheta} = \dfrac{\vartheta - \vartheta_0}{\vartheta_0}, \qquad \kappa_s(\vartheta) = \kappa_s^* - \kappa_s^{**}\overline{\vartheta}, \qquad \kappa_0(\vartheta) = \kappa_0^* - \kappa_0^{**}\overline{\vartheta},$

$$\delta(\vartheta) = \delta^* - \delta^{**}\overline{\vartheta}, \qquad \beta(\vartheta) = \beta^* - \beta^{**}\overline{\vartheta},$$

(2.28) $\xi^F = \xi^{F*} - \xi^{F**} \left\langle \left(\dfrac{\|\mathbf{L_v \xi}\| - \|\mathbf{L_v \xi}_c\|}{\|\mathbf{L_v \xi}_c\|}\right)^{m_F} \right\rangle,$

(2.29) $\mathbf{p} = \dfrac{\partial f}{\partial \boldsymbol{\tau}}\bigg|_{\boldsymbol{\xi}=\text{const}} \left(\left\|\dfrac{\partial f}{\partial \boldsymbol{\tau}}\right\|\right)^{-1} = \dfrac{1}{[2J_2' + 3A^2(\text{tr}\boldsymbol{\tau})^2]^{1/2}}[\boldsymbol{\tau}' + A\text{tr}\boldsymbol{\tau}\boldsymbol{\delta}],$

and f denotes the potential function [4, 18, 19, 29], κ is the isotropic work–hardening–softening function [15, 19], $\boldsymbol{\tau}'$ represents stress deviator, J_1, J_2' are the first and the second invariants of Kirchhoff stress tensor and deviatoric part of the Kirchhoff stress tensor, respectively, $A = 2(n_1 + n_2(\boldsymbol{\xi} : \boldsymbol{\xi})^{1/2})$, ξ^{F*} can be thought as a quasi-static fracture porosity and $\|\mathbf{L_v \xi}_c\|$ denotes equivalent critical velocity of microdamage. Notice, that Eq. (2.28) reflects experimental fact, that the fracture porosity changes for fast processes. Such an approach is consistent with the, so called, cumulative fracture criterion [2, 6], which assumes the existence of critical time needed for saturation of microdamage to its fracture limit.

4. For microdamage mechanism we take the additional assumptions [3, 4]:
  • increment of the microdamage state is coaxial with the principal directions of stress state,
  • only positive (tension) principal stresses induces the growth of the microdamage,

we have

(2.30) $\dfrac{\partial g^*}{\partial \boldsymbol{\tau}} = \left\langle \dfrac{\partial \widehat{g}}{\partial \boldsymbol{\tau}} \right\rangle \left\| \left\langle \dfrac{\partial \widehat{g}}{\partial \boldsymbol{\tau}} \right\rangle \right\|^{-1}, \qquad \text{and} \qquad \widehat{g} = \dfrac{1}{2}\boldsymbol{\tau} : \mathcal{G} : \boldsymbol{\tau},$

(2.31) $\Phi^g \left(\dfrac{I_g}{\tau_{eq}(\boldsymbol{\xi}, \vartheta, \in^p)} - 1\right) = \left(\dfrac{I_g}{\tau_{eq}} - 1\right)^{m_g},$

  where

(2.32) $\tau_{eq} = c(\vartheta)(1 - (\boldsymbol{\xi} : \boldsymbol{\xi})^{1/2}) \ln \dfrac{1}{(\boldsymbol{\xi} : \boldsymbol{\xi})^{1/2}}$

$$\cdot \{2\kappa_s(\vartheta) - [\kappa_s(\vartheta) - \kappa_0(\vartheta)] F(\xi_0, \boldsymbol{\xi}, \vartheta)\}, \qquad c(\vartheta) = \text{const.},$$

$$(2.33) \qquad F = \left(\frac{\xi_0}{1 - \xi_0} \frac{1 - (\boldsymbol{\xi} : \boldsymbol{\xi})^{1/2}}{(\boldsymbol{\xi} : \boldsymbol{\xi})^{1/2}} \right)^{\frac{2}{3}\delta} + \left(\frac{1 - (\boldsymbol{\xi} : \boldsymbol{\xi})^{1/2}}{1 - \xi_0} \right)^{\frac{2}{3}\delta},$$

and

$$(2.34) \qquad I_g = \bar{b}_1 J_1 + \bar{b}_2 (J_2')^{1/2} + \bar{b}_3 (J_3')^{1/3}.$$

$\bar{b}_i$ $(i = 1, 2, 3)$ are the material parameters, J_3' is the third invariant of deviatoric part of the Kirchhoff stress tensor.

Now, taking into account the postulates for microdamage evolution, and assuming that tensor $\mathcal{G}$ can be written as a symmetric part of the fourth order unity tensor $\mathcal{I}$ [10]

$$(2.35) \qquad \mathcal{G} = \mathcal{I}^s, \qquad \mathcal{G}_{ijkl} = \frac{1}{2} \left(\delta_{ik} \delta_{jl} + \delta_{il} \delta_{jk} \right),$$

we can write the explicit form of the growth function $\widehat{g}$ as

$$(2.36) \qquad \widehat{g} = \frac{1}{2} \left(\tau_I^2 + \tau_{II}^2 + \tau_{III}^2 \right).$$

The gradient of $\widehat{g}$ with respect to the stress field gives us the following matrix representation of a tensor describing the anisotropic evolution of microdamage

$$(2.37) \qquad \frac{\partial \widehat{g}}{\partial \boldsymbol{\tau}} = \begin{bmatrix} g_{11} \tau_I & 0 & 0 \\ 0 & g_{22} \tau_{II} & 0 \\ 0 & 0 & g_{33} \tau_{III} \end{bmatrix}.$$

In (2.37) $\tau_I, \tau_{II}, \tau_{III}$ are the principal values of Kirchhoff stress tensor.

It can be noted, that the definition of the threshold stress for microcrack growth function τ_{eq} indicates that the growth term in evolution function for microdamage is active only after nucleation whereas before nucleation we have infinite threshold $\lim_{\boldsymbol{\xi} \to \mathbf{0}} \tau_{eq} = \infty$.

5. For temperature evolution Eq. (2.19) we consider the following relation

$$(2.38) \qquad \mathbf{k} = \boldsymbol{\tau}.$$

3. Numerical aspects and some examples

The main purpose of the HSM modeling and computations is to estimate properly the forces that act in the cutting machine tools. It helps to design the elements of HSM-machines. For description of the material itself and particularly its thermo-plastic behaviour we use the constitutive relations of different order of

complexity. More or less these properties combines the physical observation with mathematical elegance. One of the fundamental problem is to estimate properly (identify) the constitutive parameters placed in the mathematical structure. This could be the topic of a separate study. So, let us allow to use the set of parameters which describe the same mild steel for three used formulations (JC, RK, Perzyna models). We will show the results obtained for different speed of machining and different friction coefficient between specimen and the tool. The other numerical aspects also will be stressed.

3.1. Orthogonal cutting – geometry, boundary and initial conditions

The analysed HSM set up is presented in Fig. 2. The tool is rigid and its geometry is described be an exterior angle equal $7°$ and the fillet radius equal 3 μm. The dimensions of the machined sample (3D) are length 2000 μm, height 200 μm and out of plane thickness 5 μm.

The boundary conditions on a sample are applied at the bottom, front and rear surfaces, while rigid tool can move in horizontal direction only with constant velocity 12 ms^{-1}. The initial conditions assume room temperature.

a)

b)

angle = 7^0
filled radius = 3 μm

rigid
tool

length = 0.002 m = 2000 μm
high = 0.0002 m = 200 μm
out of plane thickness = 0.000005 m = 5 μm

v=12 m/s
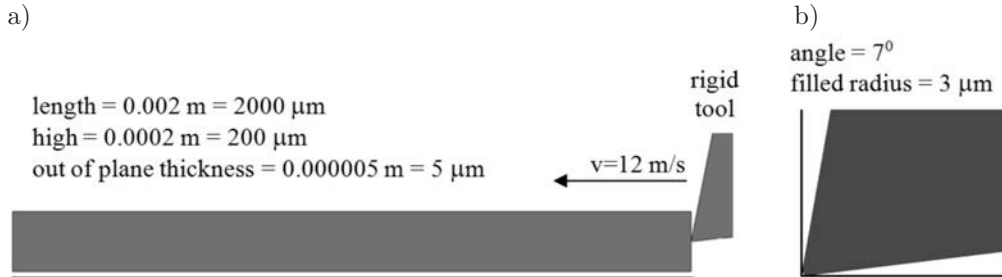
FIG. 2. a) Configuration of the High Speed Machining; b) Geometry of the rigid tool.

3.2. Material models implementation

The discussed material models are all implemented in Abaqus/Explicit commercial finite element code. While Johnson–Cook model is pre-implemented in Abaqus/Explicit code, the two other, namely Rusinek–Klepaczko and Perzyna's viscoplasticity models are added to the software by taking advantage of a user subroutine VUMAT, which is coupled with Abaqus system [1]. Let us mention that the Abaqus/Explicit utilises central-difference time integration rule along with the diagonal ("lumped") element mass matrices. The details concerning implementation of Rusinek–Klepaczko and Perzyna's viscoplasticity models as Abaqus subroutine VUMAT can be found in [27, 34] and [31], respectively.

3.3. Material parameters for ES mild steel

The material parameters for the ES mild steel for Johnson–Cook, Rusinek–Klepaczko and Perzyna's viscoplasticity type models are collected in Tables 1–3, respectively.

Table 1. Material parameters for ES mild steel – Johnson–Cook model.

$T_{\text{melt}} = 1600$ K	$\beta = 0.9$	$\rho = 7800$ kg/m^3	$C_p = 470$ J/kgK
$\alpha = 10^{-5}$ K^{-1}	$E = 210$ GPa	$\nu = 0.3$	$A = 57.27$ MPa
$B = 479.93$ MPa	$n = 0.316$	$C = 0.0362$	$\dot{\varepsilon}_0 = 0.001$ 1/s
$T_0 = 300$ K	$m = 0.28$		

Table 2. Material parameters for ES mild steel – Rusinek–Klepaczko model.

$T_m = 1600$ K	$\beta = 0.9$	$\rho = 7800$ kg/m^3	$C_p = 470$ J/kgK
$\alpha = 10^{-5}$ K^{-1}	$E_0 = 210$ GPa	$\nu = 0.3$	$\theta^* = 0.59$
$T_0 = 300$ K	$B_0 = 591.6$ MPa	$n_0 = 0.285$	$\varepsilon_0 = 0.018$
$D_1 = 0.48$	$\nu_{CR} = 0.2$	$\sigma_0^* = 406.3$ MPa	$m^* = 2.8$
$D_2 = 0.19$			

Table 3. Material parameters for ES mild steel – Perzyna's type viscoplasticity model.

$\lambda = 121.154$ GPa	$\mu = 80.769$ GPa	$\rho_{\text{Ref}} = 7800$ kg/m^3	$m_g = 1$
$c = 0.067$	$b_1 = 0.02$	$b_2 = 0.5$	$b_3 = 0$
$\xi^{F^*} = 0.36$	$\xi^{F^{**}} = 0$	$m_F -$	$|L_\upsilon \xi_c| - $ s^{-1}
$\delta^* = 6.0$	$\delta^{**} = 1.4$	$T_m = 2.5$ µs	$m_{pl} = 0.14$
$\kappa_s^* = 430$ MPa	$\kappa_s^{**} = 97$ MPa	$\kappa_0^* = 317$ MPa	$\kappa_0^{**} = 71$ MPa
$\beta^* = 11.0$	$\beta^{**} = 2.5$	$n_1 = 0$	$n_2 = 0.25$
$\chi^* = 0.8$	$\chi^{**} = 0.1$	$\theta = 10^{-5}$ K^{-1}	$c_p = 470$ J/kgK

3.4. Numerical results

Johnson–Cook model

Plane stress versus plane stress conditions

During the orthogonal cutting (HSM) three dimensional block (volume) is cut and for simulation of this process the solid elements are used together with proper description of boundary conditions to assure the plane strain conditions. We do not use directly plane strain elements because for 3D cases the general contact algorithm is more efficient.

It is the reason that in our simulations we have only one layer of finite elements with out of plane thickness 5 μm. For this thickness and for element size 10 μm in plane XY we present the distribution of equivalent stresses for two conditions (plane strain and plain stress), Fig. 3.
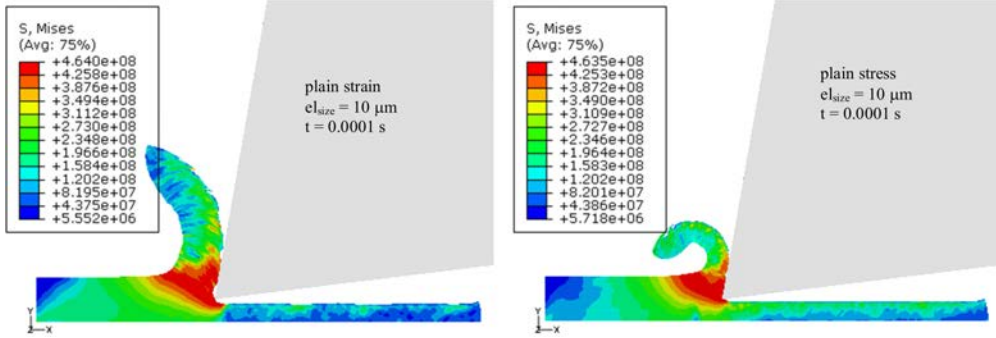

Fig. 3. The maps of equivalent stresses for plain stress and plane strain cases; element size is 10 μm.

The state of deformation presented in Fig. 3 for two cases shows that more real formation of chip is using plane strain condition [13, 30]. For plane stress condition the large influence is played by the strain tensor component perpendicular to the plane XY. It leads to fast failure of the material (the chip is very thin). The force which acts on the tool during cutting process is similar in both considered cases. The average forces are 0.45 N for both cases for 5 μm thickness of the model. The force is proportional to the thickness and for example if the thickness is 1000 μm (1 mm) the cutting force is equal to 90 N $(0.45 \text{ N} \cdot 1000 \text{ μm}/5 \text{ μm})$.

Finite elements size

Previous simulations and analyzes lead to the conclusion that in the case of orthogonal cutting (HSM) the plane strain condition should be used (all nodes of the cut material have blocked displacement U3). The important aspect of numerical modelling with strain and strain rate hardening but with temperature softening (adiabatic condition), is the description of the mesh size dependency that proofs the well-possedness of the IBVP. It is presented in this section.

The maps of equivalent stresses and strains for different element sizes: 20 μ m, 15 μm, 10 μm are presented in Fig. 4. The used FE meshes are shown above the HMH stresses maps. The average cutting forces for one layer of finite elements (5 μm) are of order 0.7 N, 0.5 N and 0.45 N. The important is also that for larger finite elements the higher fluctuations are obtained, see Fig. 5. In the next simulations we will use the smallest finite elements size (10 μm). The real localization zones in the described processes are approximately of the dimensions of the smallest used elements (10 μm).
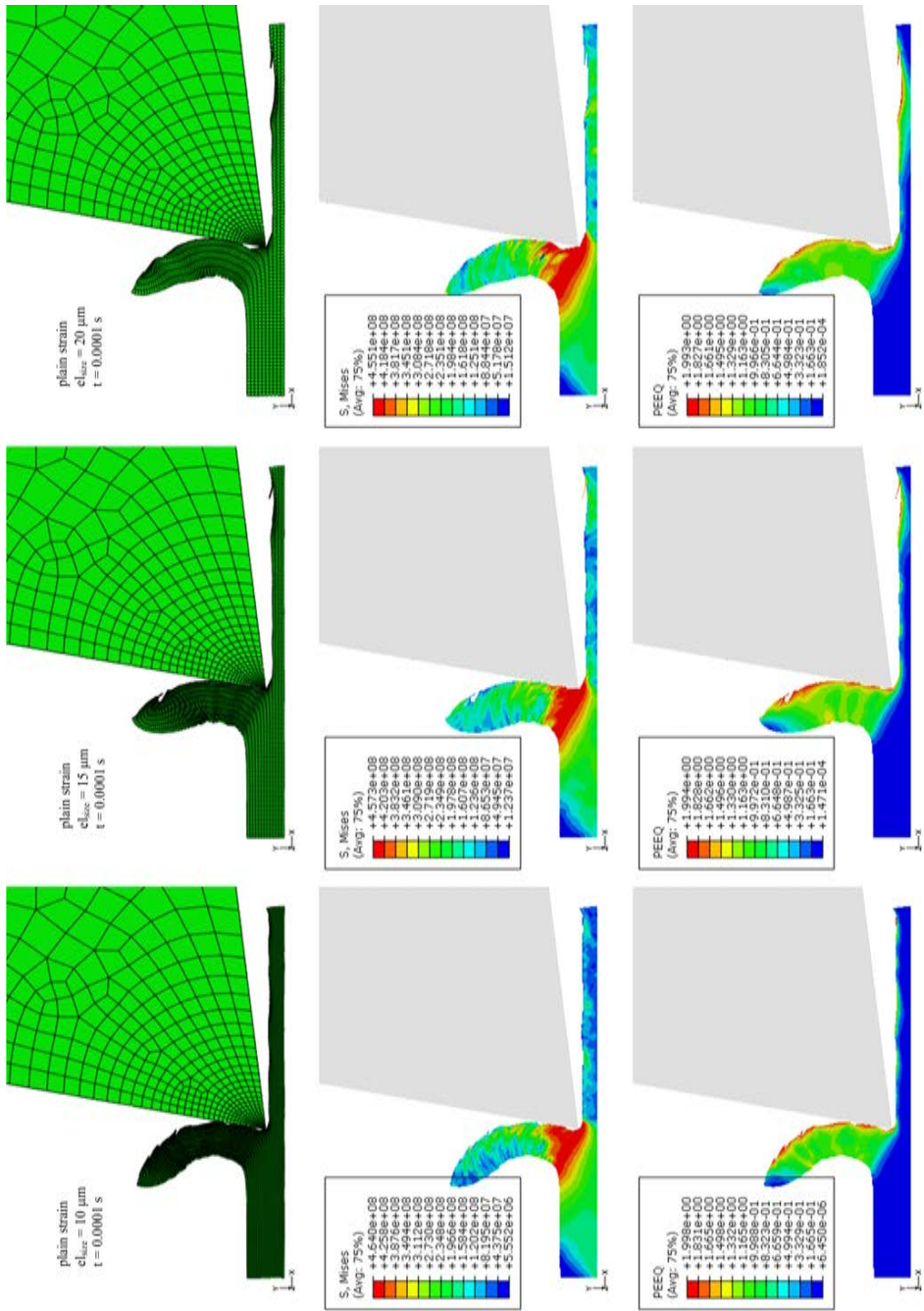
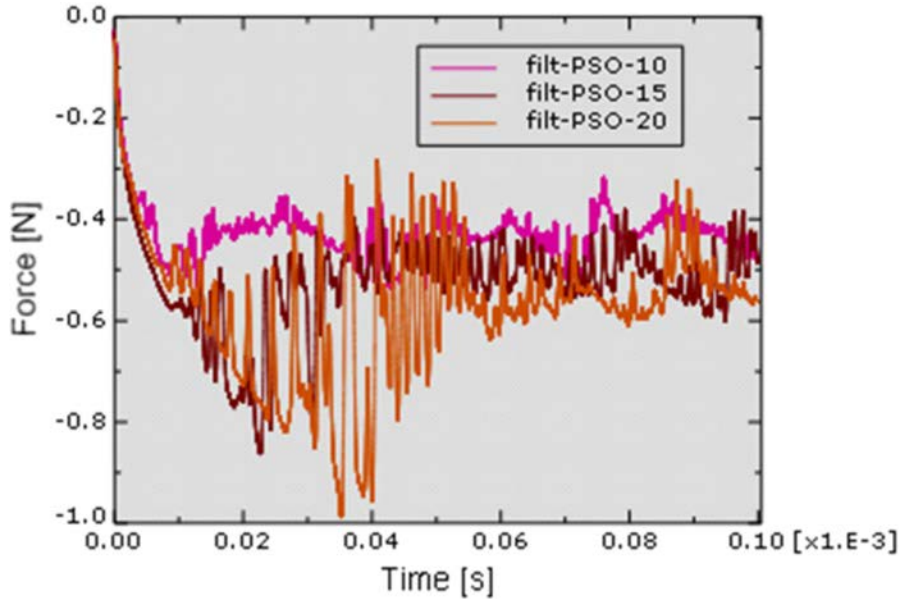FIG. 4. The equivalent stresses and strains maps for different element size: 10 μm, 15 μm, 20 μm.

Fig. 5. The cutting force for different element sizes.

Friction

The influence of friction coefficient is significant. Figure 6 present the maps of the equivalent stresses, strains and temperatures for different friction coefficients (0.3, 0.1). We can observe the deformation and chip formation processes. For smaller friction coefficient the chip behaves in more ductile way, however the maximal temperature and plastic deformation are of the same order. The maximum value of stresses, strains and temperatures are close for two considered cases. The cutting force is smaller for friction coefficient 0.1 (0.4 N) than for friction coefficient 0.3 (0.45 N).

Rectangle versus triangle finite elements

It is well known that the different shapes of the elements can introduce to the IBVP a kind of numerical anisotropy (dispersion effect). The most cases this drives to uncorrected estimation of the localization zones. In this section the influence of alignment for two types of finite elements (rectangle and triangle) is presented. The density of finite elements is similar (el_{size} = 10 μm) in both cases and only element type (el_{type}) is different.

The deformation of the models is different. In model with the triangle elements the partitioning of the chip is clearly visible while visible using rectangle finite element the chip is continuous. Additionally, the cutting forces were compared and in case of triangle elements the average force is about 0.7 N (for el_{type} = rectangle it is 0.45 N).
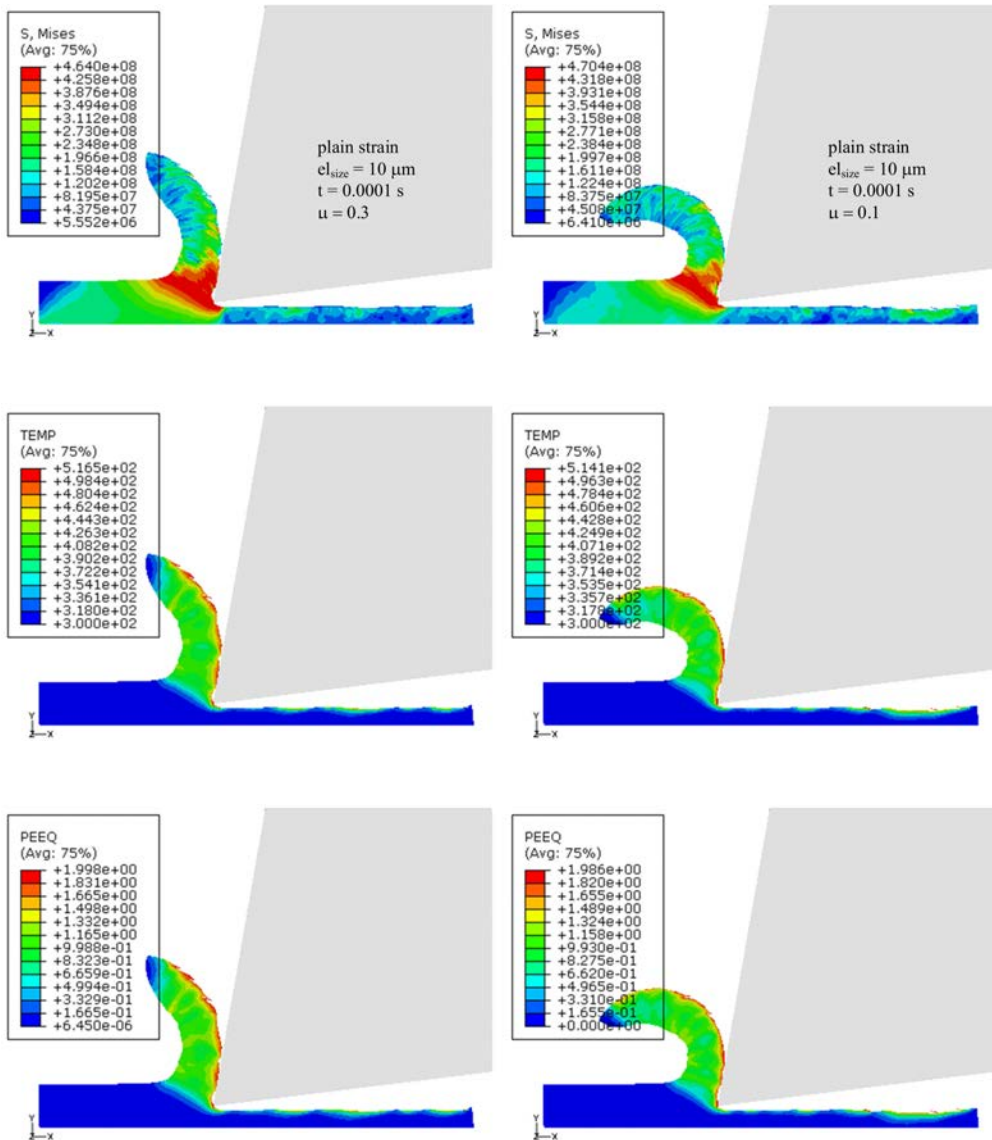
FIG. 6. The maps of equivalent stresses, temperatures and strains for two friction coefficients: 0.3 and 0.1 for fixed element size 10 μm.

The different effects in JC modelling

The next considered aspect is the influence of constitutive parameters on failure mode and chip formation. Four cases were taken into account, see Fig. 8. In Fig. 8a the all effects are included it means, strain hardening, strain rate hardening and temperature softening. The results (Fig. 8a) are presented also in Fig. 6a and Fig. 7a. In Fig. 8b, the yield stress is independent of strains,
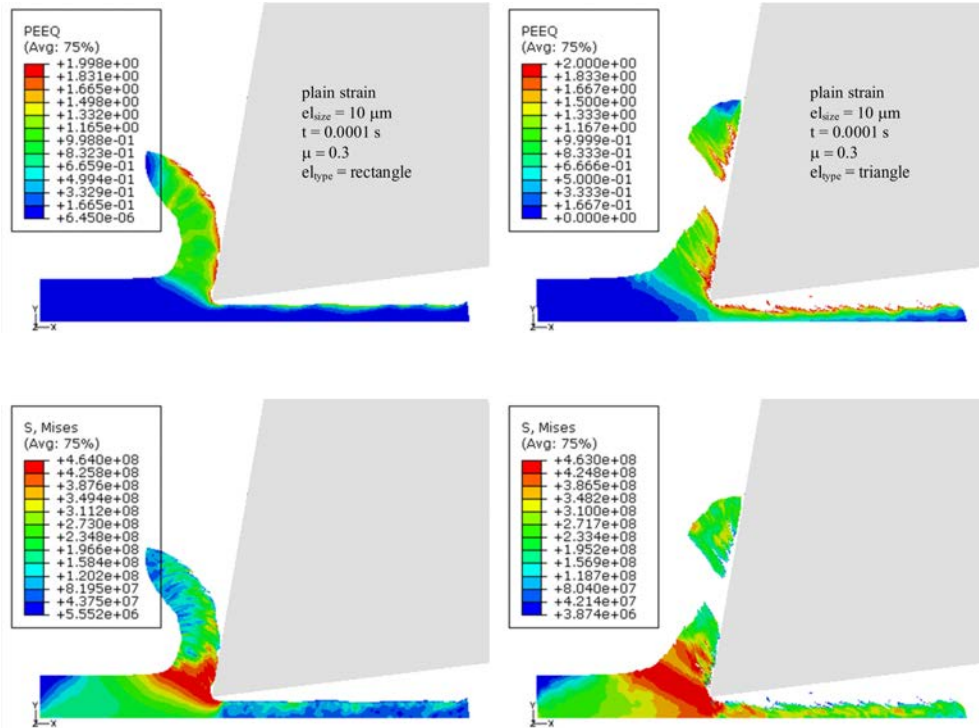
FIG. 7. The maps of equivalent plastic strains, stresses, for two mesh alignments.

strain rates and temperatures. The Fig. 8c presents the situation where yield stress depends only on strain. The last map of equivalent strains presents the case where yield stress is a function of strain (hardening) and temperature (softening), see Fig. 8d. In Fig. 8e the plot of cutting forces for all cases is presented. In case A the average cutting force is 0.45 N, for case B it is only 0.07 N, for case C the cutting force is 0.6 N but for case D it is 0.3 N. The results show the effects of taking into consideration some parts of Eq. (2.1) into JC model and also using the simplifications.

The depth of cut

As the last effect in this section the depth of the cut is discussed. Previous results took into account only one depth (100 μm). Now we present the results for the other depth cut equal (50 μm). The comparison of the obtained results is presented in Fig. 9. In Fig. 9c one can observe the history of the cutting force for two depths of cut. The force varies in time but the average cutting force for cut depth 100 μm is 0.45 N and for 50 μm is 0.27 N. These results are also in agreement with other reported simulations and with laboratory test for other materials [13, 30].
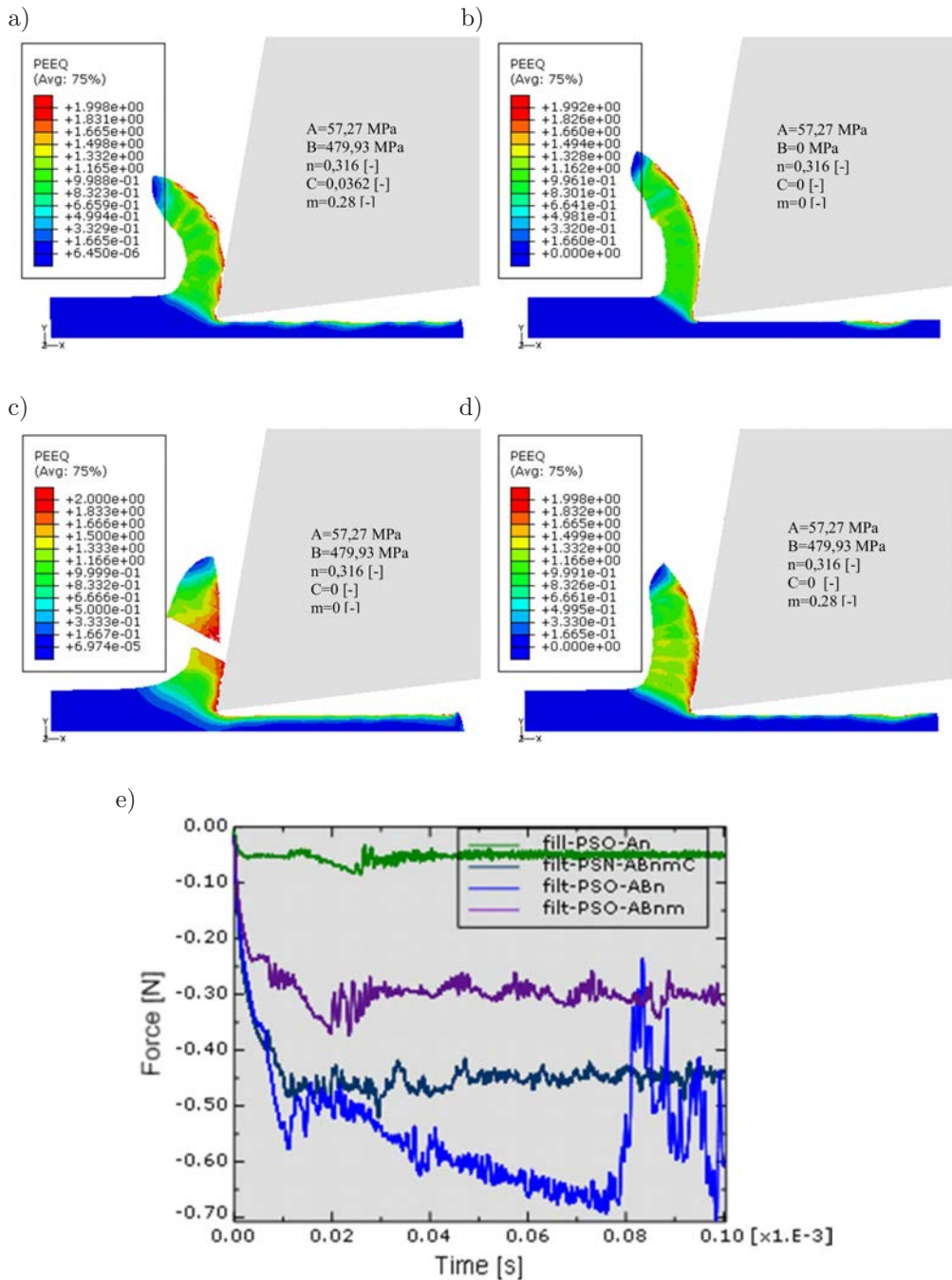
a)

b)

c)

d)

e)

FIG. 8. The maps of equivalent strains for four cases with different effects: a) all effects are included, b) independent yield stress only, c) yield stress with strain hardening, d) yield stress with strain hardening and temperature softening, e) the plot of cutting forces for the all studied cases.
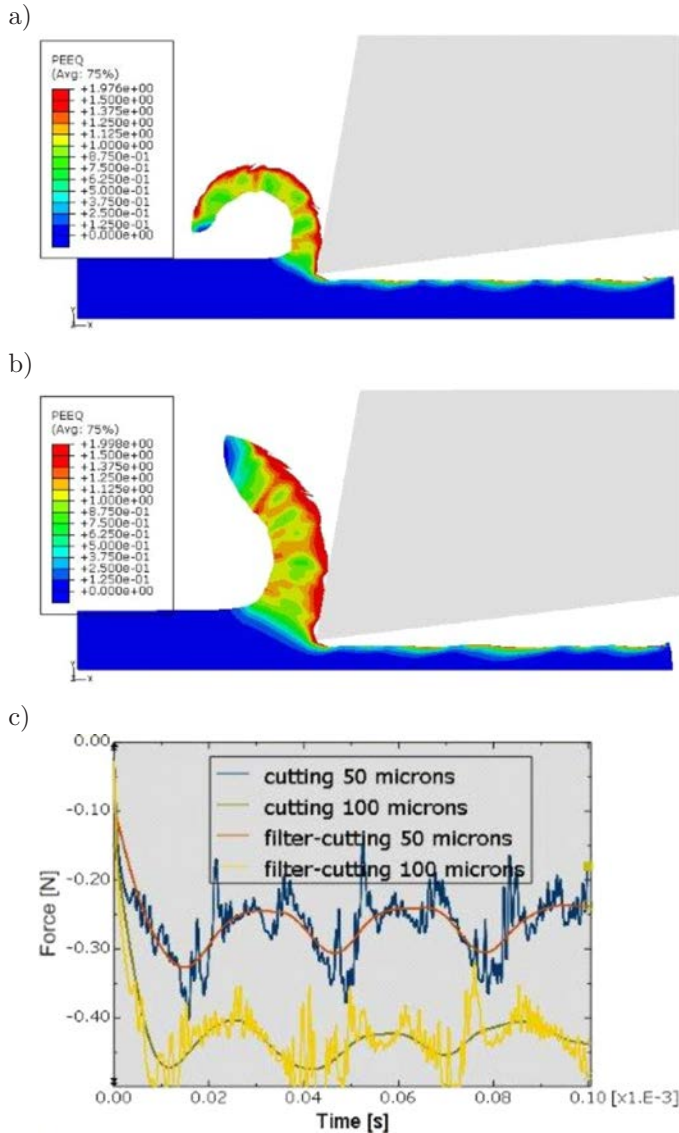
a)

b)

c)

FIG. 9. The maps of equivalent strains for different depth cut cases with: a) 50 μm,
b) 100 μm, c) cutting force comparison.

Rusinek-Klepaczko model. The depth of the cut is discussed also in this
section for RK model. These results, as before, took into account two depths
(50 μm and 100 μm). The comparison of the obtained results is presented in
Fig. 10. In Fig. 10c one can observe the history of the cutting force for two
cut depths. The force varies in time but the average cutting force for cut depth
100 μm is 0.55 N (in case of JC it was 0.45 N) and for 50 μm is 0.35 N (in case
of JC it was 0.27 N).

a)

b)

c)
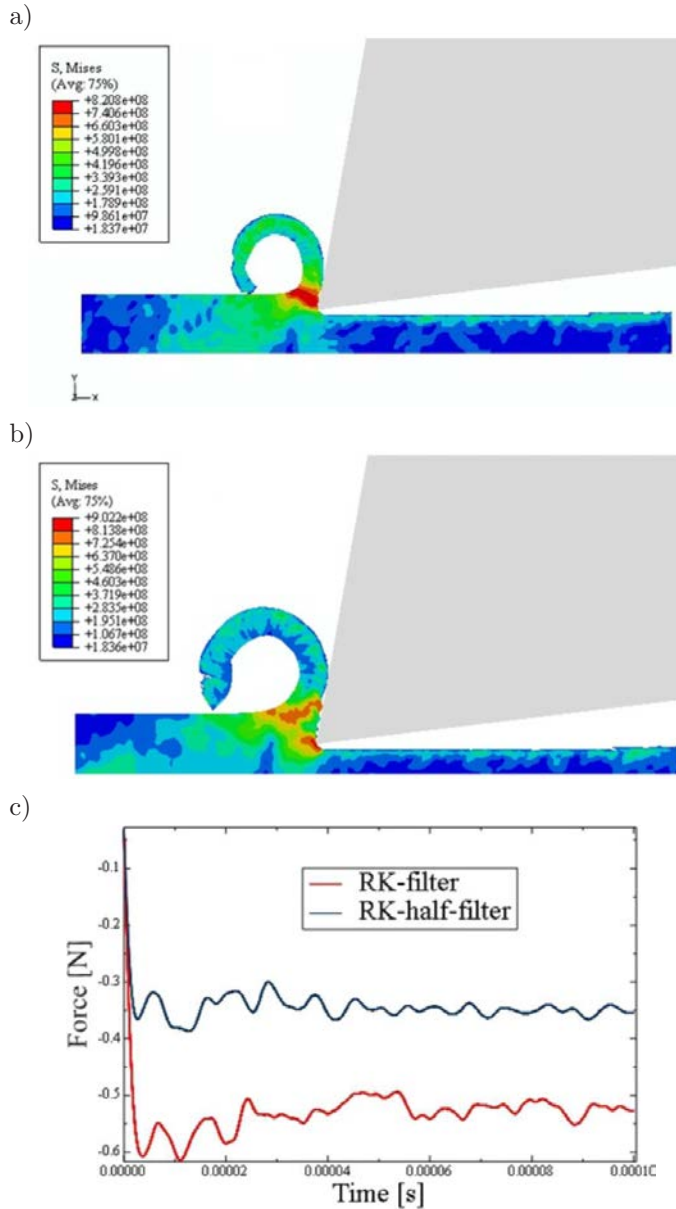
Fig. 10. The maps of equivalent strains for two cases with different depth of cut: a) 50 μm, b) 100 μm, c) cutting force comparison.

Perzyna's type viscoplasticity model. Finally, the results obtained using Perzyna's type viscoplasticity model for the machined sample are discussed. Through the analyses we have accepted mesh refinement or alignment like in previous examples, so we have used C3D8R element with approximate size 10 μm. As a case study we have consider two cut depths (50 μm and 100 μm) and

we have repeated the computations with and without adaptive mesh technique (Arbitrary Lagrangian Eulerian (ALE) adaptive mesh technique cf. [1]).

Let us point out, that the analysis with Perzyna's type viscoplasticity model needs additional assumption concerning the initial microdamage state (distribution of ξ_0), what has a serious consequences on final macrodamage evolution [32]. Because of lack of detailed experimental data, we have assumed in all analyses homogenous and isotropic initial microdamage state, such that initial porosity was in every material point equal $\|\xi_0\| = 6 \cdot 10^{-4}$ [14]. Notice, that anisotropy introduced by ξ involves full spatial modeling.

Global response

The comparison of the reaction on a tool for cutting depths 50 μm and 100 μm including influence of ALE adaptive mesh technique is presented in Fig. 11. Recall, that those results are the most important for machinery designers. Like for previously presented results an average force that acts on the tool for cutting depth 50 μm is around 0.3 N while for cutting depth 100 μm reaches approximately 0.6 N. Notice, that like in a real experiment resultant force changes due to chip sticking to the tool. Nevertheless this small influence of ALE technique on global level is more distinct on local one concerning e.g. chip geometry and its damage as will be shown in the following.
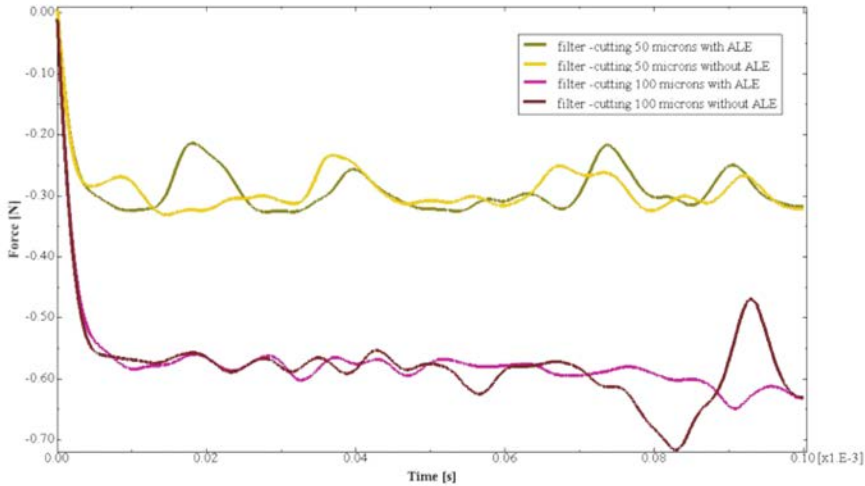

FIG. 11. Comparison of the reaction on the tool for cutting depth 50 μm and 100 μm including influence of ALE adaptive mesh technique.
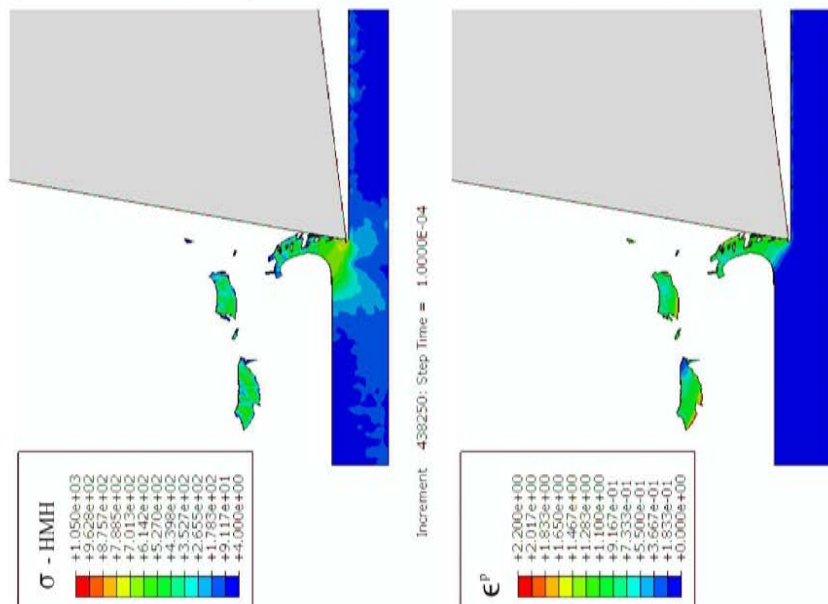
Local response

The comparison of the HMH stresses, the equivalent viscoplatic strains, the temperature and the porosity maps for cutting depths 50 μm and 100 μm at time instant 10^{-4} s are presented in Figs. 12 and 13, respectively. For both cases
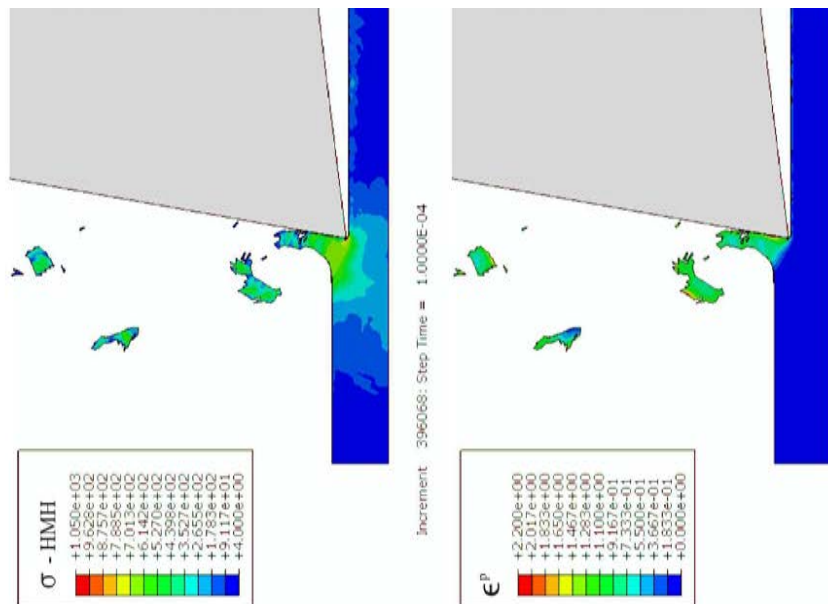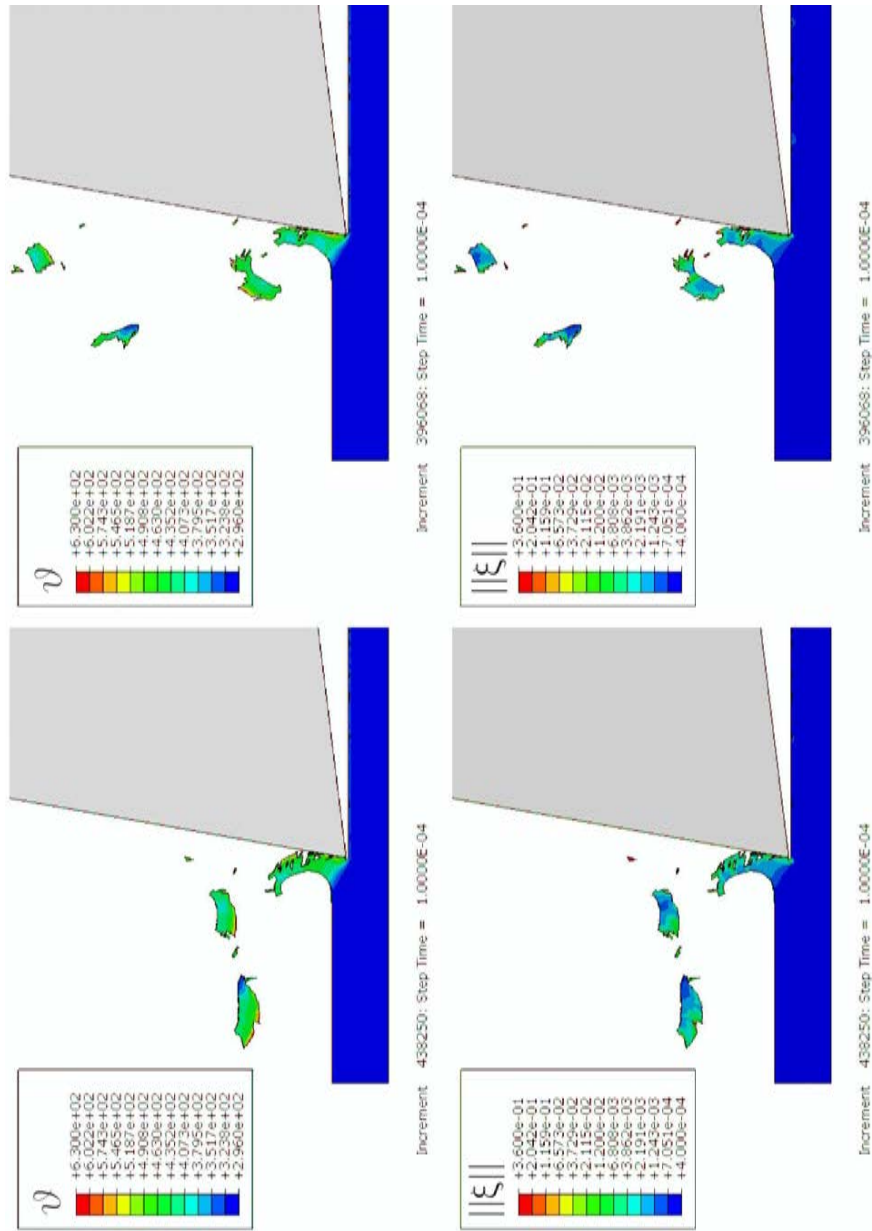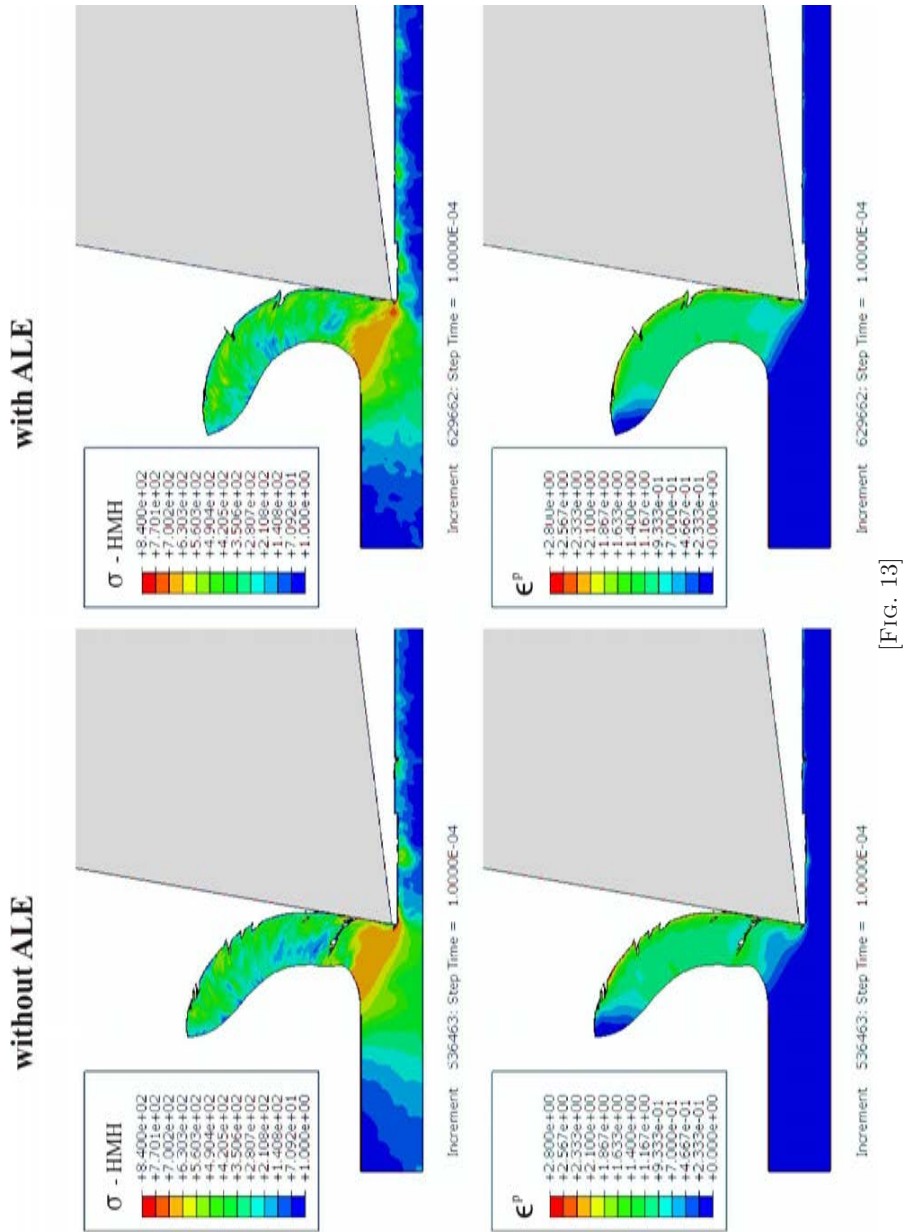
[Fig. 12]

FIG. 12. The comparison of the HMH stresses, the equivalent viscoplastic strains, the temperature and the porosity maps for cutting depth 50 μm at time instant 10^{-4} s, without and with ALE technique in left and right columns, respectively.

[Fig. 13]

Fig. 13. The comparison of the HMH stresses, the equivalent viscoplatic strains, the temperature and the porosity maps for cutting depth 100 μm at time instant 10^{-4} s, without and with ALE technique in left and right columns, respectively.
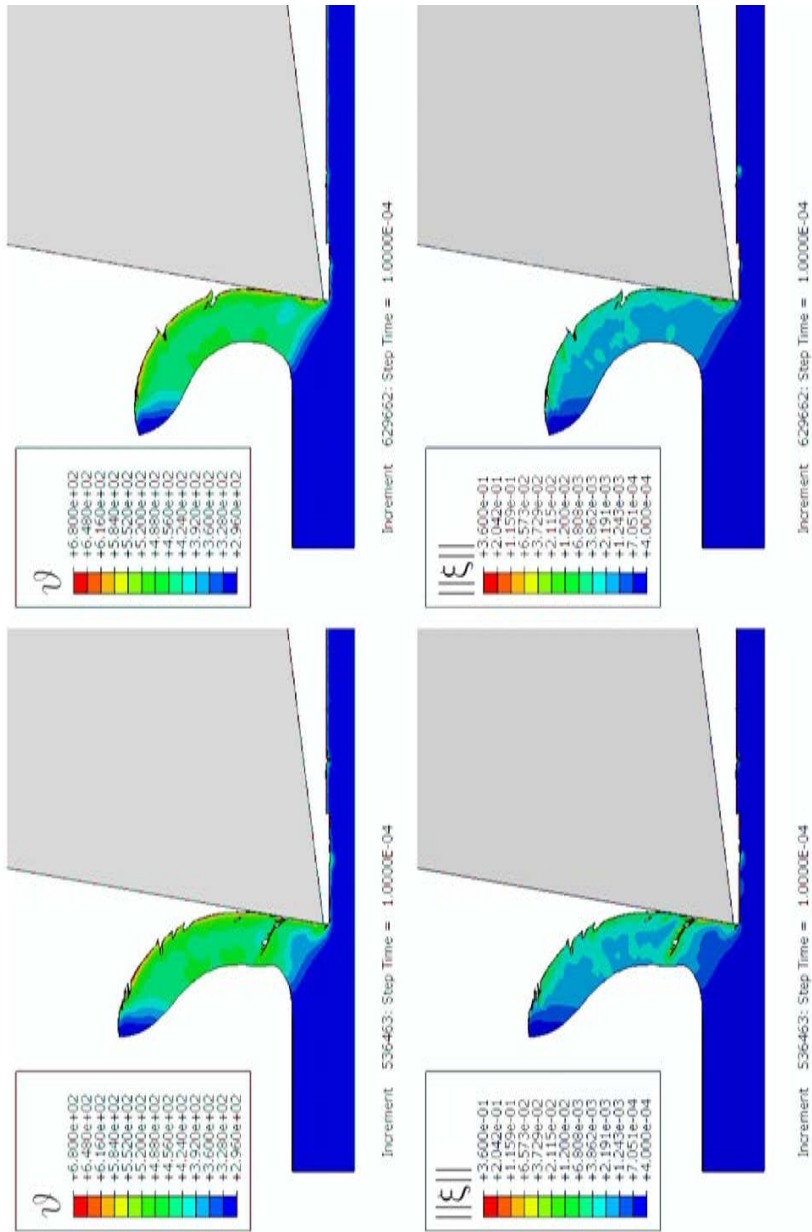
we present the results obtained without and with using ALE technique. Notice, that for easier analysis of the maps, each time in rows we use legend with the same upper and lower bounds.

The first notice from Figs. 12 and 13 is that the chip geometry is different. For the case of cutting depth 50 μm it is hard to interpret the difference due to severe fragmentation of the chip, however for cutting depth 100 μm we observe that without ALE technique the chip bends less and there exist a macrodamage. Let us emphasise that fragmentation is due to shear banding.

The maps in Figs. 12 and 13 show that the distribution of presented quantities is very similar. We observe that locally (at a tool tip) the HMH stresses reaches around 1000 MPa, the equivalent viscoplatic strains can obtain even 2.8 and the temperature in close to 680 K. Moreover, the local strain rates (what is not presented graphically), described by the tensor $\mathbf{d}$ (Eq. (2.15), are of the order $4 \cdot 10^6 \text{ s}^{-1}$. Notice, that cutting of local extrema in plots we have similar results as for previously presented results concerning J-C and RK material models.

4. Conclusions

The comparison of the results that describe the distribution of stresses and strains, influence of mesh refinement and alignment also using ALE formulation as well as friction between tool and specimen were discussed for accepted three constitutive models (JC, RK, and Perzyna). The obtained results differ in details but qualitatively gave very similar effects in particular in estimation of forces that acts on tools.

Using of one of the above constitutive relations in numerical simulations depends significantly on the possibility of proper identification of material parameters. Let us stress at the end that in practical engineering easier accepted are simpler relations (those which have smaller amount of parameters), sometimes not so strongly physically and mathematically proven.

Acknowledgment

References

1. *Abaqus Version 6.10ef1 Theory Manual.* 2010.

2. Campbell J.D., *The dynamic yielding of mild steel*, Acta Metallurgica, **1**, 6, 706–710, 1953.

3. DORNOWSKI W., *Influence of finite deformations on the growth mechanism of microvoids contained in structural metals*, Archives of Mechanics, **51**, 1, 71–86, 1999.

4. GLEMA A., ŁODYGOWSKI T., SUMELKA W., PERZYNA P., *The numerical analysis of the intrinsic anisotropic microdamage evolution in elasto-viscoplastic solids*, International Journal of Damage Mechanics, **18**, 3, 205–231, 2009.

5. JOHNSON G.R., COOK W.H., *A constitutive model and data for metals subjected to large strains, high strain rates and high temperatures*, [in:] Proceedings of the sevens international symposium on ballistics, pp. 541–547, The Hague, The Netherlands, 1983.

6. KLEPACZKO J.R., *Behavior of rock like materials at high strain rates in compression*, International Journal of Plasticity, **6**, 415–432, 1990.

7. KLEPACZKO J.R., RUSINEK A., RODRÍGUEZ–MARTÍNEZ J.A., PĘCHERSKI R.B., ARIAS A., *Modelling of thermo-viscoplastic behaviour of DH-36 and Weldox 460-E structural steels at wide ranges of strain rates and temperatures, comparison of constitutive relations for impact problems*, Mechanics of Materials, **41**, 5, 599–621, 2009.

8. LEE E.H., *Elastic-plastic deformation at finite strain*, ASME Journal of Applied Mechanics, **36**, 1–6, 1969.

9. ŁODYGOWSKI T., *Theoretical and numerical aspects of plastic strain localization*, D.Sc. Thesis, Publishing House of Poznan University of Technology, **312**, 1996.

10. ŁODYGOWSKI T., GLEMA A., SUMELKA W., *Anisotropy induced by evolution of microstructure in ductile material*, [in:] 8th World Congress on Computational Mechanics (WCCM8), 5th European Congress on Computational Methods in Applied Sciences and Engineering (ECCOMAS 2008), Venice, Italy, June 30 – July 5 2008.

11. ŁODYGOWSKI T., PERZYNA P., *Localized fracture of inelastic polycrystalline solids under dynamic loading process*, International Journal Damage Mechanics, **6**, 364–407, 1997.

12. ŁODYGOWSKI T., PERZYNA P., *Numerical modelling of localized fracture of inelastic solids in dynamic loading process*, International Journal for Numerical Methods in Engineering, **40**, 4137–4158, 1997.

13. MOLINARI A., MUSQUAR C., SUTTER G., *Adiabatic shear banding in high speed machining of Ti-6Al-4V: experiments and modeling*, International Journal of Plasticity, **18**, 443—459, 2002.

14. NEMES J.A., EFTIS J., *Several features of a viscoplastic study of plate-impact spallation with multidimensional strain*, Computers and Structures, **38**, 3, 317–328, 1991.

15. NEMES J.A., EFTIS J., *Constitutive modelling of the dynamic fracture of smooth tensile bars*, International Journal of Plasticity, **9**, 2, 243–270, 1993.

16. PERZYNA P., *The constitutive equations for rate sensitive plastic materials*, Quarterly of Applied Mathematics, **20**, 321–332, 1963.

17. PERZYNA P., *Fundamental problems in viscoplasticity*, Advances in Applied Mechanics, **9**, 243–377, 1966.

18. PERZYNA P., *Constitutive modelling for brittle dynamic fracture in dissipative solids*, Archives of Mechanics, **38**, 725–738, 1986.

19. PERZYNA P., *Internal state variable description of dynamic fracture of ductile solids*, International Journal of Solids and Structures, **22**, 797–818, 1986.

20. PERZYNA P., *Instability phenomena and adiabatic shear band localization in thermoplastic flow process*, Acta Mechanica, **106**, 173–205, 1994.

21. PERZYNA P., *The thermodynamical theory of elasto-viscoplasticity*, Engineering Transactions, **53**, 235–316, 2005.

22. PERZYNA P., The thermodynamical theory of elasto-viscoplasticity accounting for microshear banding and induced anisotropy effects. Mechanics, **27**, 1, 25–42, 2008.

23. RUSINEK A., KLEPACZKO J.R., *Shear testing of a sheet steel at wide range of strain rates and a constitutive relation with strain-rate and temperature dependence of the flow stress*, International Journal of Plasticity, **17**, 1, 87–115, 2001.

24. RUSINEK A., RODRÍGUEZ–MARTÍNEZ J.A., *Thermo-viscoplastic constitutive relation for aluminium alloys, modeling of negative strain rate sensitivity and viscous drag effects*, Materials and Design, **30**, 10, 4377–4390, 2009.

25. RUSINEK A., RODRÍGUEZ–MARTÍNEZ J.A., ARIAS A., *A thermo-viscoplastic constitutive model for FCC metals with application to OFHC copper*, International Journal of Mechanical Sciences, **52**, 2, 120–135, 2010.

26. RUSINEK A., RODRÍGUEZ–MARTÍNEZ J.A., KLEPACZKO J.R., PĘCHERSKI R.B., *Analysis of thermo-visco-plastic behaviour of six high strength steels*, Materials and Design, **30**, 5, 1748–1761, 2009.

27. RUSINEK A., ZAERA R., *Finite element simulation of steel ring fragmentation under radial expansion*, International Journal of Impact Engineering, **34**, 799—822, 2007.

28. RUSINEK A., ZAERA R., KLEPACZKO J.R., *Constitutive relations in 3-D for a wide range of strain rates and temperatures: Application to mild steels*, International Journal of Solids and Structures, **44**, 17, 5611–5634, 2007.

29. SHIMA S., OYANE M., *Plasticity for porous solids*, International Journal of Mechanical Sciences, **18**, 285–291, 1976.

30. SIMA M., ÖZEL T., *Modified material constitutive models for serrated chip formation simulations and experimental validation in machining of titanium alloy Ti-6Al-4V*, International Journal of Machine Tools and Manufacture, **50**, 943—960, 2010.

31. SUMELKA W., *The Constitutive Model of the Anisotropy Evolution for Metals with Microstructural Defects*, Publishing House of Poznan University of Technology, Poznań, Poland, 2009.

32. SUMELKA W., ŁODYGOWSKI T., *The influence of the initial microdamage anisotropy on macrodamage mode during extremely fast thermomechanical processes*, Archive of Applied Mechanics, **81**, 12, 1973–1992, 2011.

33. TRUESDELL C., NOLL W., *The non-linear field theories of mechanics*, [in:] Handbuch der Physik, vol. III/3, Springer-Verlag, Berlin, S. Flügge [Ed.], 1965.

34. ZAERA R., FERNÁNDEZ–SÁEZ J., *An implicit consistent algorithm for the integration of thermoviscoplastic constitutive equations in adiabatic conditions and finite deformations*, International Journal of Solids and Structures, **43**, 6, 1594–1612, 2006.